PERGAMON

Journal of Structural Geology 22 (2000) 1385–1393

JOURNAL OF STRUCTURAL GEOLOGY

www.elsevier.nl/locate/jstrugeo

Enhancement of fluid permeability during shear deformation of a synthetic mud

Shuqing Zhang*, Stephen F. Cox

Research School of Earth Sciences, The Australian National University, Canberra, ACT 0200, Australia

Received 5 November 1999; accepted 15 May 2000

Abstract

This study concerns the effect of stress paths on permeability and permeability anisotropy in a synthetic mud at conditions where cataclastic flow is dominant. The synthetic mud is composed of 10 wt.% montmorillonite, 40 wt.% illite, and 50 wt.% silt-sized quartz. In the experiments where the mud was first consolidated at 90 MPa effective pressure (p_e) and then also sheared at 90 MPa p_e, permeability decreased continuously with increasing shear displacement; subsequent shear deformation at 30 MPa and 20 MPa effective pressure resulted in permeability increases. The permeabilities parallel to and across the mud layer are similar during shear deformation at 90 MPa p_e and remain so during shear deformation at lower p_e. In the experiments where shear deformation commenced at 30 MPa p_e after an initial consolidation at 90 MPa, permeability increased significantly with increasing displacement. Combined effects of reducing mean effective stress and shear sliding result in permeability enhancement up to two orders of magnitude. The permeability parallel to the shear direction is one order of magnitude higher than that across the shear plane.

Our shear deformation experiments at high pressures confirm the importance of stress path on the evolution of fluid permeability during shear deformation. The experimental results clearly indicate that to effectively enhance permeability and to channel fluids along shear zones in wet sediments, mean effective stress needs to be less than several tens of MPa.

1. Introduction

There is strong circumstantial evidence indicating that large fluid flux in accretionary prisms can occur along fault zones, particularly, décollement zones (Gieskes et al., 1990; Taylor and Leonard, 1990; Knipe et al., 1986; Moore et al., 1991; Moore and Vrolijk, 1992; Brückman et al., 1997; Fisher and Zwart, 1997; Zwart et al., 1997). Hydrogeological simulations of fluid flow patterns and fluid pressure distribution in the Barbados and the Oregon prisms suggest that the permeability along the décollement zone should be more than three orders of magnitude higher than in the surrounding sedimentary matrix (Screaton et al., 1990; Henry and Wang, 1991). Such enhancement of fluid permeability in shear zones was observed by Arch and Maltman (1990) during permeability measurements at ambient conditions on experimentally deformed sediments. Permeability increases of up to two orders of magnitude were found in the direction parallel to the shear zone and were attributed to development of preferred alignment of clay fabrics during deformation. However, the result of Arch and Maltman (1990) has been challenged by a number of subsequent shear sliding experiments (Brown and Moore, 1993; Brown et al., 1994; Dewhurst et al., 1996a,b; Zhang et al., 1999a,b). These experiments unambiguously showed that shear deformation of unlithified sediments in the compactive deformation regime results in permeability decreases in the shear zones relative to the surrounding wall rocks and that permeability anisotropy associated with the development

* Corresponding author. Tel: +61-2-6249-5167; fax: +61-2-6279-8253.

E-mail address: shuqing.zhang@anu.edu.au (S. Zhang).

0191-8141/00/$ - see front matter
PII: S0191-8141(00)00065-1

of preferred shape fabrics of clays is not large enough to explain channelised fluid flow along shear zones. More recently, Bolton et al. (1998) suggested that differences in the effective stress history may explain the apparent contradiction among existing experimental results. Their analysis, using 'critical state' soil mechanics and uniaxial compression experiments at low confining pressures ($\sim$1 MPa), clearly demonstrated that deformation of 'overconsolidated' sediments enhances permeability. This result may have profound significance in understanding the dynamic nature of permeability in active fault zones given that the amount of unlithified materials and fluid pressure can vary both spatially and temporally.

The experiments of Bolton et al. (1998) were conducted under very low mean effective stress conditions and they simulated near-surface deformation of wet sediments where porosity is high (>33%) and particulate flow is presumably the dominant deformation mechanism (Knipe, 1986). Clearly, application of this result to fault zones situated further landward of the deformation front of accretionary prisms, is critically dependent on understanding the interactions of stress with porosity and permeability under high mean effective stresses where porosity is low and cataclastic flow is predominant. One critical question is whether or not the evolution of porosity and permeability during shear deformation under low mean effective stress conditions is similar to that at higher mean effective stress conditions.

We have deformed a synthetic mud at mean effective stresses ranging from 15 to 150 MPa. We have measured permeability both parallel to and across the experimental fault plane. In the present paper, we will first show how the effective stress history influences the evolution of permeability and permeability anisotropy during shear deformation. We will then examine the individual roles of stress path, fluid pressure and clay shape fabrics in the overall evolution of permeability and permeability anisotropy.

2. Experimental details

A synthetic mud was prepared by mechanically mixing 10 wt.% montmorillonite, 40 wt.% illite, and 50 wt.% silt-sized quartz (Brown and Moore, 1993). A 1-mm-thick layer of water-presaturated mud paste was placed in the 45° saw cut between either two permeable ceramic blocks (permeability $\sim 10^{-13}$ m^2) or two impermeable stainless steel blocks with permeable ceramic slots as ports for fluid input and output (Fig. 1a and b). Fluid permeability parallel to and across the mud layer was measured with these two specimen assemblies, respectively. To inhibit sliding along the piston–mud layer interfaces, regular shallow grooves 50 μm deep and spaced 500 μm apart, were produced on the sliding surfaces of the stainless steel blocks by electron discharge machining (EDM). The mud layer and the sliding blocks were surrounded by an inner Teflon jacket of about 0.25 mm wall thickness and by an outer annealed copper jacket of about 0.25 mm wall thickness. Tests indicate that, at effective pressures (confining pressure minus pore fluid pressure) higher than about 10 MPa, there is no fluid flow between the copper–Teflon–specimen interfaces.

Isostatic loading and shear deformation experiments were performed in an argon-gas-medium, triaxial deformation apparatus (Paterson, 1990). The argon-confining medium was separated from water pore fluid by the copper jacket and rubber O-ring seals. During each experiment, the confining pressure was first raised to about 10 MPa. The pore fluid system was then simultaneously evacuated from the downstream and upstream ends of the specimen using a vacuum pump. Doubly deionized water was then pumped into the

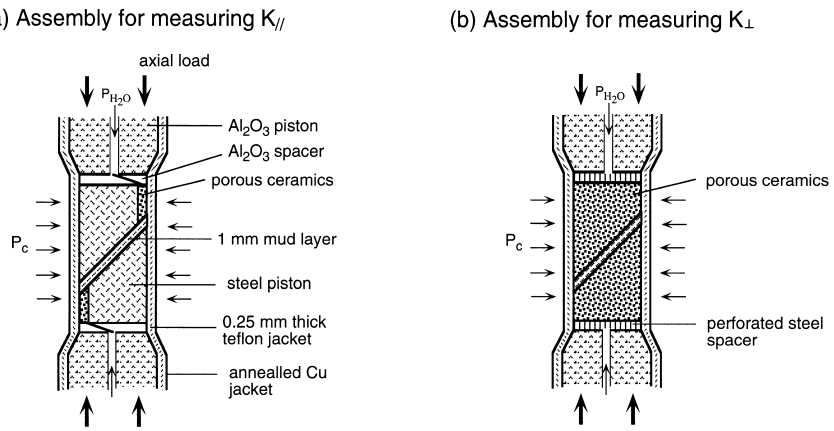

Fig. 1. Specimen assembly for measuring permeability. (a) Fluid flow parallel to the experimental fault; and (b) fluid flow across the fault. The loading piston is about 12.75 mm in diameter and 27 mm long.

pore spaces from both ends of the specimen. Further isostatic loading of the specimen was completed by increasing water pore pressure and confining pressure approximately following hydrostatic and lithostatic pressure gradients, respectively. Subsequent shear deformation of the mud layer was achieved by loading the specimen assembly uniaxially at a constant displacement rate of 3.4×10^{-4} mm/s, or a shear strain rate of about 1×10^{-3} s^{-1}. The axial load was measured with an internal load cell to an accuracy of better than 0.1 kN. Calculation of the shear strength of the mud layer has taken into account the strength of the Teflon jacket and annealed copper (Handin and Hager, 1958). The axial displacement was measured with an external LVDT and was corrected for the distortion of the specimen assembly and apparatus.

Changes in porosity within the mud layer during isostatic loading and shear deformation were determined by monitoring changes of the mud layer thickness using the displacement LVDT and by measuring the volume of fluid flowing in or out of the specimen at constant fluid pressure using a volumometer (Zhang et al., 1994). The relative error in measuring porosity by monitoring the specimen length change is about 8%. The minimum pore volume change detectable by the volumometer is about 0.005 mm^3, which corresponds to a porosity change about of 0.003%. The 'steady-state flow' method was used for permeability measurements by applying a constant pressure difference between each end of the mud layer. Permeability was calculated using Darcy's law. The imposed fluid pressure differences varied from 0.5 to 10 MPa and the measured water flow rates ranged from 0.1 to 0.00005 mm^3/s. During each stage of isostatic loading, fluid flow through the mud sample was commenced after the 'time-dependent' porosity changes stabilised. Further porosity changes during the period of permeability measurement are negligible (fluid flow rate for permeability measurements $\gg$ 10 times of the volumetric strain rate due to porosity change). During shear deformation, permeability was measured after shear sliding was halted and porosity change is negligible. The reproducibility for permeability measurement is within a factor of about 1.2.

Two stress paths were used in deforming the synthetic mud layer (Fig. 2). In both stress paths, the first stage involves progressive, isostatic loading (consolidation) to 90 MPa effective pressure with a confining pressure of 150 MPa and a pore water pressure of 60 MPa. In the first case (Path 1, a–b–d–f_1–g_1–h), after the initial compaction, the effective pressure was reduced to 30 MPa by increasing water pore pressure to 120 MPa. An effective pressure of 30 MPa was maintained during the first 3-mm shear sliding; it was then decreased to 20 MPa for further shear sliding. Alternatively, shear deformation commenced at an effective pressure of 90 MPa after the initial compaction (Path 2, a–b–c–e–f_2–g_2–h). After 2 mm and 4 mm sliding, the effective pressure was reduced to 30 MPa and 20 MPa, respectively. The two stress paths are represented as a–b–d–f_2–g_2–h and a–b–c–e–f_1–g_1–h, respectively, in the porosity–log mean effective stress space (Fig. 2b). The mean effective stress (σ_m) is defined as $(\sigma_1 + 2\sigma_3)/3 - P_f$, where P_f is the pore fluid pressure, σ_1 and σ_3 are the maximum and the least principal stress, respectively. During isostatic consolidation, σ_1 is equal to σ_3. Therefore, mean effective stress is equal to effective pressure. Along each stress path, two experiments were conducted during which permeabilities respectively parallel to the mud layer and across it were measured as a function of shear displacement.

3. Results

3.1. Mechanical behaviour

The displacement–mean effective stress curves are shown in Fig. 3. Scattering of the data, for example, at

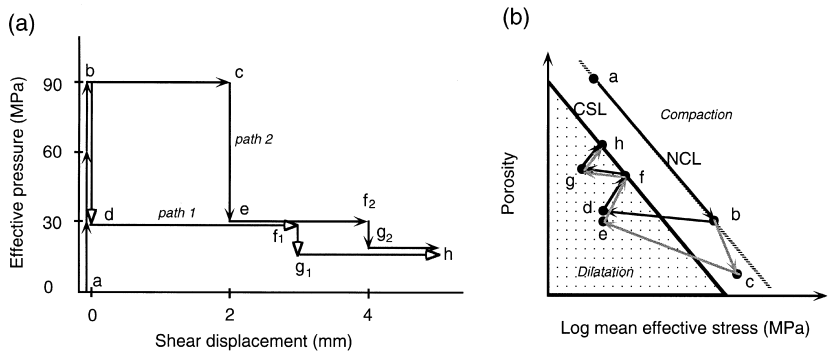

Fig. 2. Two effective stress paths used in the present study. Path 1: a–b–d–f_1–g_1–h, and Path 2: a–b–c–e–f_2–g_2–h. (a) Effective pressure as a function of shear displacement. (b) Porosity vs. log mean effective stress (modified from Bolton et al., 1998). NCL and CSL represent Normal Consolidation Line and Critical State Line, respectively.

displacement of 2.9 mm and 3.6 mm of run 4049, is caused by the stress relaxation when shear sliding was halted for permeability measurements. In the two experiments where shear deformation commenced at an effective pressure of 30 MPa (4046, 4047), deformation is characterised by an early stage of nearly steady-state sliding followed by a slight strain hardening. Continuous strain hardening occurred in the two runs (4048, 4049) where shear sliding started at 90 MPa effective pressure.

3.2. Evolution of porosity and permeability

3.2.1. Porosity

For fluid flow parallel to the fault plane, the evolution of porosity for the two stress paths is shown in Fig. 4(a) and (b), respectively. For fluid flow across the fault plane, the evolution of porosity for the two stress paths is shown in Fig. 4(c) and (d), respectively. Porosity is plotted against mean effective stress (σ_m). The two stress paths, a–b–d and a–b–c–e–f–g–h, are defined in Fig. 2. Porosity decreases with increasing mean effective stress during isostatic consolidation (a–b) and shear deformation at an effective pressure of 90 MPa (b–c). During deformation at 30 MPa effective pressure, there is a slight decrease in porosity measured for flow parallel to the fault. However, there is a slight increase in porosity, when measured for flow across the fault. Porosity clearly increases during deformation at effective pressure of 20 MPa (g–h). At the same mean effective stress, porosity is slightly higher in isostatically consolidated specimens than in sheared samples.

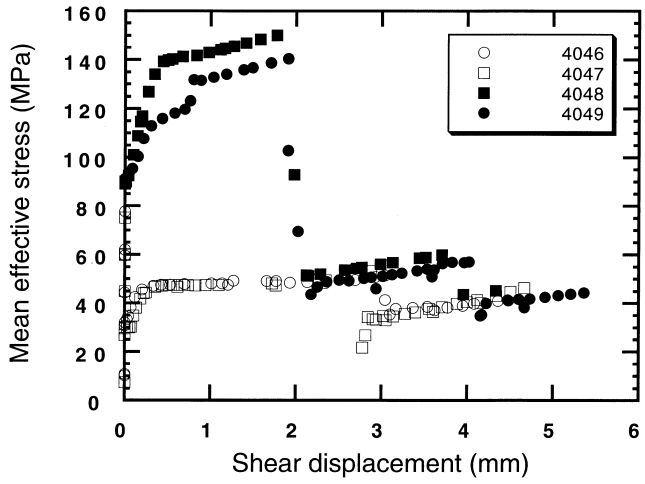

Fig. 3. Mean effective stress vs. shear displacement. Those values at 0 shear displacement represent isostatic consolidation. All experiments were conducted at a constant axial displacement rate of 3.4×10^{-4} mm/s. Experiment 4046: stress path a–b–d–f_1–g_1–h, fluid flow parallel to the fault plane. Experiment 4047: stress path a–b–d–f_1–g_1–h, fluid flow across the fault plane. Experiment 4048: stress path a–b–c–e–f_2–g_2–h, fluid flow across the fault plane. Experiment 4049: stress path a–b–c–e–f_2–g_2–h, fluid flow parallel to the fault plane.

3.2.2. Permeability

The effect of stress path on the evolution of permeability is shown in Fig. 5(a) and (b). For specimens consolidated at 90 MPa effective pressure and then sheared at 90 MPa (Fig. 5a), permeability initially decreases with shear deformation and permeabilities parallel to and across the mud layer (fault plane) become similar. Further displacement at effective pressures of 30 MPa and 20 MPa results in permeability enhancement. However permeability anisotropy remains minimal. For specimens where shear deformation commenced at an effective pressure of 30 MPa after an initial consolidation at 90 MPa (Fig. 5b), permeability mostly increases with increasing shear sliding and permeability anisotropy of half to one order of magnitude was maintained throughout shear deformation.

3.2.3. Porosity–permeability relationship

Over a range of porosity from 25% to about 5%, log permeability is linearly related to porosity (Fig. 6). The linear relationship suggests that most pores are fully connected.

3.2.4. Stress dependency of permeability

In Fig. 7, permeabilities during consolidation and shear sliding are plotted as a function of mean effective stress. Assuming an exponential relationship between permeability (k) and mean effective stress (σ_n): $k = k_0 \exp(-\gamma\sigma_n)$ (Rice, 1992; David et al., 1994), we obtained a mean stress dependency of permeability (γ) about 0.035 MPa^{-1} for consolidation (isostatic pressing). The values of γ during pore pressure increase (decrease in mean effective stress) are much lower than 0.035 MPa^{-1} (Fig. 7a and c). The exponential $k - \sigma_n$ relationship is also valid for shear deformation at an effective pressure of 90 MPa. In contrast, log permeability is non-linearly related to effective mean stress during shear sliding at effective pressures of 30 MPa and 20 MPa.

Fig. 7 also shows that at the same mean effective stress, permeability can vary by up to about one order of magnitude depending on stress history. The permeability in specimens sheared at an effective pressure of 20 MPa can be enhanced by shear deformation to a level well above that for consolidated material. Combined with the observation that sheared specimens always have lower porosity than consolidated specimens (Fig. 4), one has to conclude that some intergranular preferential flow pathways must have developed during shear deformation.

3.2.5. Microstructures

During consolidation, preferred alignments of clay shape fabric and long axes of any elongate quartz particles are sub-parallel to the shear plane. Shear deformation at effective pressures of both 90 MPa and 30–20 MPa occurred approximately uniformly across the whole gouge layer (Fig. 8a). The dominant shear texture is a foliation intersecting the fault plane at 15–20° to the fault plane. Compared with samples that underwent consolidation only (Fig. 8b), sheared samples exhibit a very strong preferred orientation of platy clay minerals, and some grain size reduction (Fig. 8c). The microstructures in sheared samples indicate that cataclastic flow is probably the predominant deformation process.

4. Discussion

The present study shows that shear deformation of wet sediments at effective pressures of 20–30 MPa leads to permeability enhancement by up to two orders of magnitude relative to their state of isostatic consolidation at 90 MPa effective pressure. Changes in fluid pressure, clay shape fabrics, and shear induced dilatancy during deformation along particular effective stress paths are important factors influencing permeability evolution in deforming mud.

4.1. Effect of fluid pressure

Via its influence on effective stress states, high fluid pressure affects fluid transport properties through elastic opening/closure of pores and inelastic pore growth/propagation (Gavrilenko and Gueguen, 1989; Walsh, 1981; Walsh and Brace, 1984). The elastic opening/closure of intergranular pores and cracks generally leads to a linear relationship between log permeability and mean effective stress (Walsh, 1981; David et al., 1994). A non-linear log permeability–mean effective stress relationship indicates pore growth. The linear relationship generally holds well in our experiments during decrease of mean effective stress by increasing fluid pressure, suggesting that there is no substantial change in pore geometry. The mean effective stress dependence of permeability is bounded by an upper value of about 0.035 MPa^{-1}, a value that is comparable with those determined for a range of clay-rich gouges (David et al., 1994; Morrow et al., 1984; Zhang et al., 1999b). This mean stress dependency of permeability implies that the development of 'sub-lithostatic' fluid pressure within fault zones itself can hardly lead to permeability increase larger than about one order of magnitude (David et al., 1994; Zhang et al., 1999b).

4.2. Effect of clay shape fabrics

Measurements of permeability both parallel to and across the fault plane show permeability anisotropy of

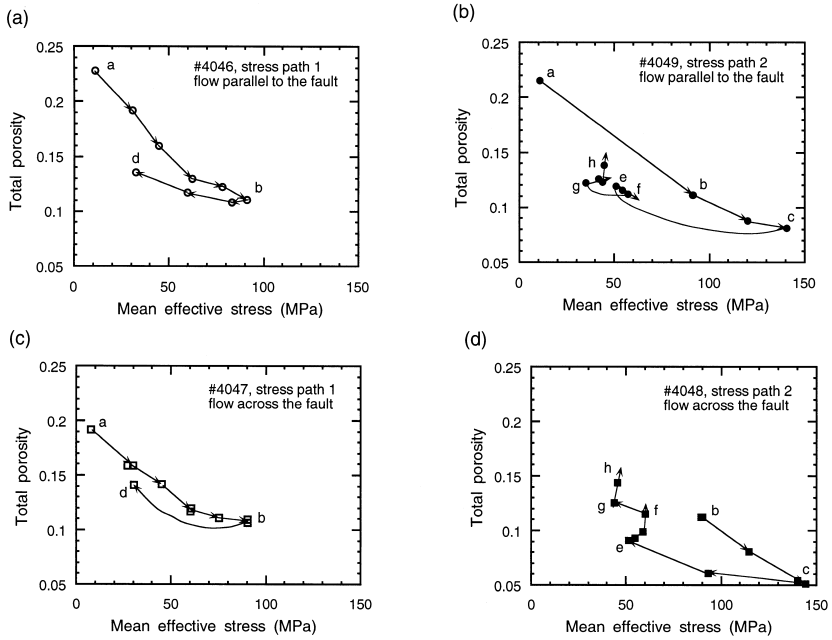

Fig. 4. Porosity as a function of mean effective stress. Letters of a, b, c, d, e, f, g and h indicate stress paths as in Fig. 2. Note that for experiments 4046 and 4047, there are no porosity measurements during shear deformation. (a) Stress path 1, fluid flow parallel to the fault, (b) stress path 2, fluid flow parallel to the fault, (c) stress path 1, fluid flow across the fault, and (d) stress path 2, fluid flow across the fault.

half to one order of magnitude during consolidation up to 90 MPa effective pressure and during shear deformation commenced at lower effective pressures. This permeability anisotropy is consistent with the preferred alignment of clay shape fabrics sub-parallel to the fault plane. The magnitude of permeability anisotropy depends on the tortuosity contrast of fluid flow paths which in turn depends on the orientation of clay fabric (Arch and Maltman, 1990) and shape geometry of individual clay flakes or aggregates (Zhang et al., 1999b). For those samples consolidated and sheared at the same effective pressure of 90 MPa initially, permeability anisotropy became minimum possibly because of more significant grain size reduction, thus reducing the tortuosity contrast of fluid flow paths.

The observed permeability anisotropy of half to one order of magnitude in the present study is consistent with previous experimental measurements by Brown and Moore (1993), Dewhurst et al. (1996a,b), and Zhang et al. (1999a,b). Permeability anisotropy larger than about 1–1.5 orders of magnitude would require the development of anisotropic shear textures such as Y shears or heterogeneous grain size reduction (Faulkner and Rutter, 1998; Zhang and Tullis, 1998; Zhang et al., 1999a).

4.3. Effect of stress paths

The evolution of porosity and permeability during deformation of a synthetic mud at high stress conditions is broadly consistent with the concept of 'critical' state soil mechanics (Wood, 1990). There, the state of deformation is represented in the porosity–log mean effective stress space (Fig. 2b). Deformation of granular materials tends to reach a steady state, which is described by the 'critical' state line along which strain accumulates without an associated change in effective stress or volume (Jones and Addis, 1986). If the stress state of the material is above the critical state line, the material will compact and permeability will decrease with deformation; whereas if the stress state is below it, material will dilate and permeability will increase.

Our deformation experiments at high pressures demonstrate that when wet sediment is deformed predominantly by cataclastic flow, and permeability can be enhanced by shear deformation along the path of reducing mean effective stress. Further, it becomes clear when comparing permeabilities at the same mean effective stress and similar shear displacements (see Fig. 5a and b), that permeabilities are similar for speci-

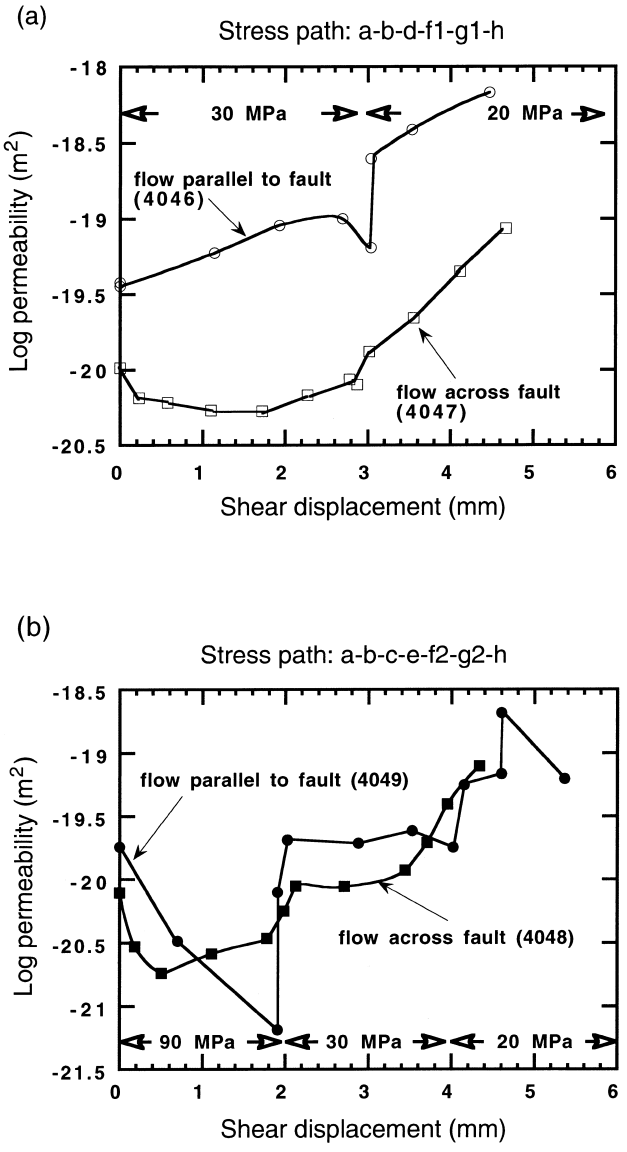

Fig. 5. Permeability evolution during shear deformation along stress paths of (a) a–b–d–f_1–g_1–h, and (b) a–b–c–e–f_2–g_2–h. The effective pressure at each stage of shear sliding is shown as 90 MPa, 30 MPa, and 20 MPa, respectively.

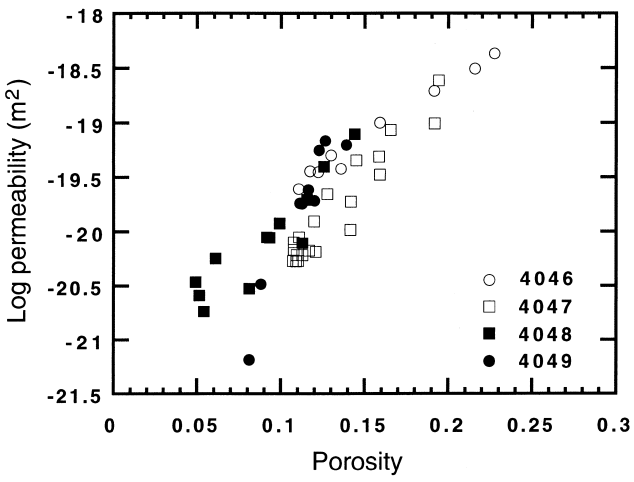

Fig. 6. Relationship between porosity and permeability.

mens deformed along the two different stress paths used in the present study. These results suggest that it is not significant whether the high fluid pressure builds up during or before shear deformation. However, the relative timings of fluid pressure increase and shear deformation have major influence on the development of permeability anisotropy.

Our experiments also show signs of development of permeability associated with grain-scale dilatancy during shear deformation at effective pressures less than several tens of MPa. This is consistent with experiments conducted under 'near-lithostatic' fluid pressures. As clearly demonstrated by Arch and Maltman (1990), Bolton et al. (1998, 1999) and Stephenson et al. (1994), development of intergranular dilatancy and microfractures during deformation of wet sediment at 'near-lithostatic' fluid pressure conditions could lead to dramatic permeability enhancement. Unfortunately, the technical difficulty for avoiding short-cut fluid flow along sample/jacket interfaces in our apparatus prevents us from examining the permeability evolution during shear deformation at effective pressures lower than 15–20 MPa.

Our results indicate that the dynamic interactions between the development of high fluid pressures and shear deformation can lead to significant permeability enhancement in shear zones in mudrock. In particular, when sheared sediments are subject to low effective pressures, deformation-induced dilatancy could effectively focus fluid expulsion along shear zones (Bolton et al., 1999; Brown et al., 1994; Tobin et al., 1994; Tobin and Moore, 1997). However, our experimental results indicate that at high effective confining pressures, aseismic shearing can be associated with progressive decrease in fault permeability, and lead to shear zones in mudrock becoming aquitards.

These results have implications for the potential coupling between fluid flow and mechanical behaviour in accretionary prisms, and the extent to which fluid flow becomes localised in actively shearing mudrocks. For example, at high pore fluid conditions, active, high permeability thrust faults will progressively drain fluid reservoirs to which they are connected. If, as a consequence of reservoir draining, fluid flow rates and fluid pressures drop, active faults will become progressively less permeable with increasing shear strain, and evolve into fault seals. Build-up of fluid pressure beneath them, in response to deeper level fluid expulsion, may ultimately promote dilatancy, shear failure, and renewed high fluid flux immediately beneath sealed faults. Complex interactions between fluid flow rates, fluid pressures and slip localisation may therefore be expected in dewatering accretionary prisms. In fact, episodic flow may be expected, and influenced by feedback between fluid pressures, reservoir draining, and slip rates.

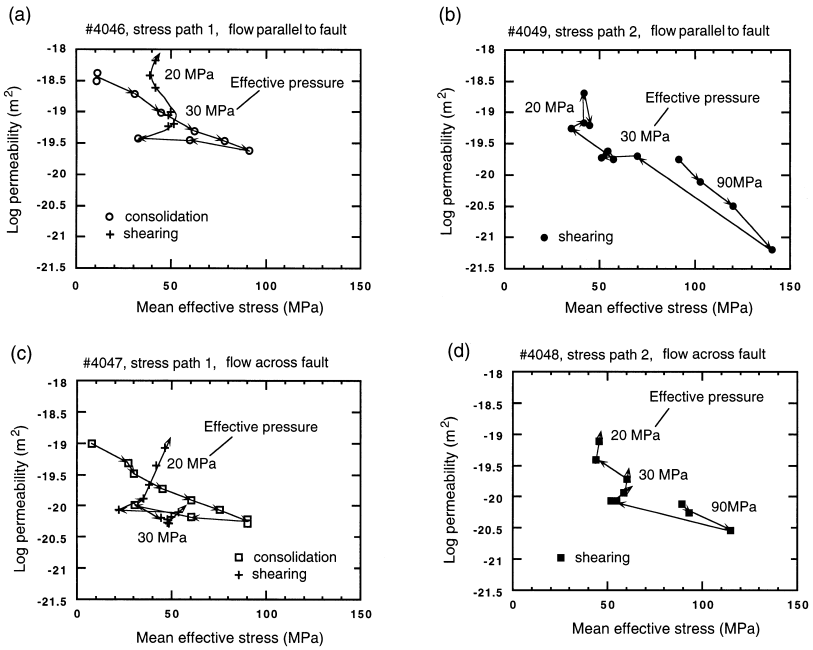

Fig. 7. Permeability as a function of mean effective stress. (a) Stress path 1, fluid flow parallel to the fault, (b) stress path 2, fluid flow parallel to the fault, (c) stress path 1, fluid flow across the fault, and (d) stress path 2, fluid flow across the fault. See Fig. 4 for corresponding porosity evolution during consolidation and shear deformation.

5. Conclusions

Isostatic consolidation and subsequent shear deformation of a synthetic mud, at conditions where cataclastic flow is dominant, lead to the following conclusions:

1. Increases in fluid pressure alone in fault zones will not lead to large permeability enhancement because of low values of stress dependency of permeability in consolidated mud.
2. Shear deformation along paths involving progressive fluid pressure increase can result in significant permeability enhancement. Substantial permeability enhancement (greater than three orders of magnitude) requires deformation to occur at effective pressures less than several tens of MPa.
3. Permeability anisotropy, of about one order of magnitude, develops when fluid pressure build-up precedes shear deformation. Enhanced permeability anisotropy in shear zones is associated with development of anisotropic shear textures.

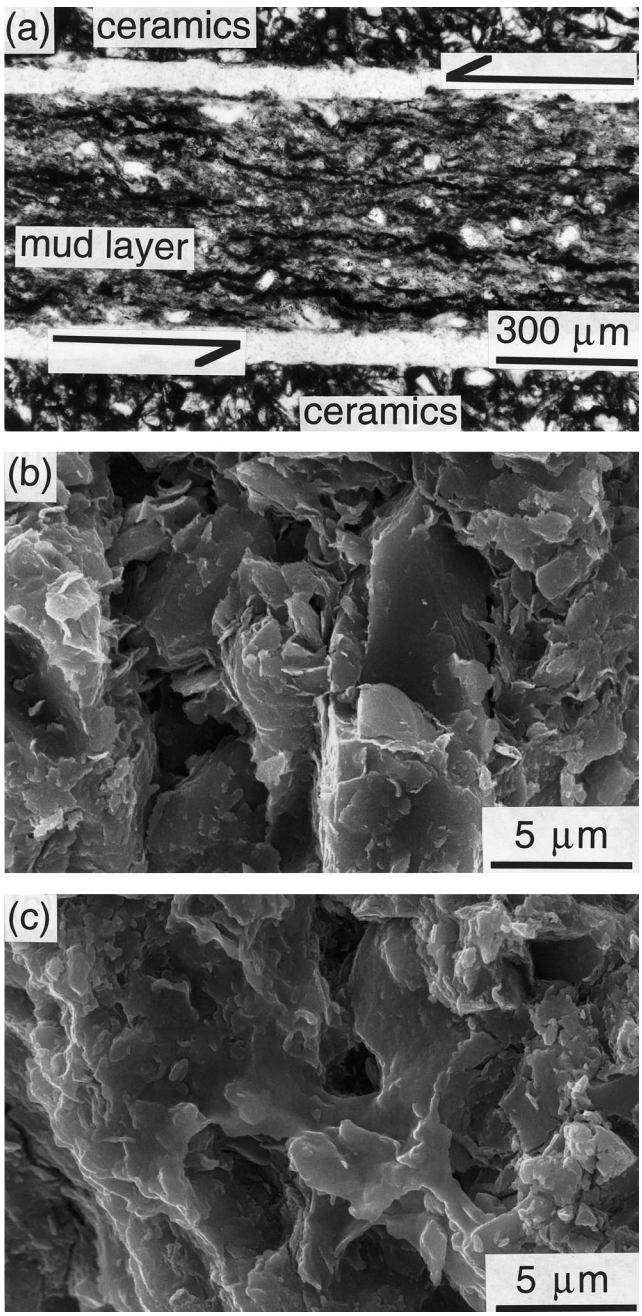

Fig. 8. Microstructures. (a) Optical micrograph of a sample sheared to a displacement about 6 mm at effective pressure of 90, 30, and 20 MPa in sequence. (b) SEM fracture surface of a sample consolidated to an effective pressure of 90 MPa. Individual clay flakes of 1–5 μm in size can be clearly seen. (c) SEM fracture surface of a sample sheared to a displacement of 6 mm at effective pressures of 90, 30, and 20 MPa in sequence. Note fine-grained clay aggregates.

References

Arch, J., Maltman, A., 1990. Anisotropic permeability and tortuosity in deformed wet sediments. Journal of Geophysical Research 95, 9035–9046.

Bolton, A.J., Clennell, M.B., Maltman, A.J., 1999. Nonlinear stress dependence of permeability: A mechanism for episodic fluid flow in accretionary wedges. Geology 27, 239–242.

Bolton, A.J., Maltman, A.J., Clennell, M.B., 1998. The importance of overpressure timing and permeability evolution in fine-grained sediments undergoing shear. Journal of Structural Geology 20, 1013–1022.

Brown, K.M., Moore, J.C., 1993. Comment on "anisotropic permeability and tortuosity in deformed wet sediments by J. Arch and A. Maltman". Journal of Geophysical Research 98, 17859–17864.

Brown, K.M., Bekins, B., Clennell, B, Dewhurst, D., Westbrook, G., 1994. Heterogeneous hydrofracture development and accretionary fault dynamics. Geology 22, 259–262.

Brückman, W., Moran, K., MacKillop, A.K., 1997. Permeability and consolidation characteristics from hole 949B, northern Barbados ridge. In: Shipley, T.H., Ogawa, Y., Blum, P., Bahr, J.M. (Eds.), Proceedings of the Ocean Drilling Program, Scientific Results, 156. College Station, TX (Ocean Drilling Program), pp. 109–114.

David, C., Wong, T-f., Zhu, W., Zhang, J., 1994. Laboratory measurements of compaction-induced permeability change in porous rocks: Implications for the generation and maintenance of pore pressure excess in the crust. Pure and Applied Geophysics 143, 425–456.

Dewhurst, D.N., Brown, K.M., Clennell, M.B., Westbrook, G.K., 1996a. A comparison of the fabric and permeability anisotropy of consolidated and sheared silty clay. Engineering Geology 42, 253–267.

Dewhurst, D.N., Clennell, M.B., Brown, K.M., Westbrook, G.K., 1996b. Fabric and hydraulic conductivity of sheared clays. Géotechnique 46, 761–768.

Faulkner, D.R., Rutter, E.H., 1998. The gas permeability of clay-bearing fault gouge at 20°C. In: Jones, G., Fisher, Q.J., Knipe, R.J. (Eds.), Faulting, Fault Sealing and Fault Flow in Hydrocarbon Reservoirs, Geological Society, London, Special Publications, 147, pp. 147–156.

Fisher, A.T., Zwart, G., 1997. Packer experiments along the décollement of the Barbados accretionary complex: measurements of in

situ permeability. In: Shipley, T.H., Ogawa, Y., Blum, P., Bahr, J.M. (Eds.), Proceedings of the Ocean Drilling Program, Scientific Results, 156. College Station, TX (Ocean Drilling Program), pp. 199–218.

Gavrilenko, P., Gueguen, Y., 1989. Pressure dependency of permeability: A model for crack rocks. Geophysical Journal International 98, 1259–1272.

Gieskes, J.M., Vrolijk, P., Blanc, G., 1990. Hydrogeochemistry, ODP Leg 110: An overview. In: Moore, J.C., Mascle, A., et al. (Eds.), Proceedings of the Ocean Drilling Program, Scientific Results, 110. College Station, TX (Ocean Drilling Program), pp. 395–402.

Jones, M.E., Addis, M.A., 1986. The application of stress path and critical state analysis to sediment deformation. Journal of Structural Geology 8, 575–580.

Handin, J., Hager, R.V., 1958. Experimental deformation of sedimentary rocks under confining pressure: Tests at high temperature. American Association of Petroleum Geologists Bulletin 42, 2892–2934.

Henry, P., Wang, C.-Y., 1991. Modeling of fluid flow and pore pressure at the toe of Oregon and Barbados accretionary wedges. Journal of Geophysics Research 96, 20109–20130.

Knipe, R.J., 1986. Deformation mechanism path diagrams for sediments undergoing lithification. In: Moore, J.C., Lundberg, N. (Eds.), Deformation in Sediments from Forearcs, Geological Society of America Memoir, 166, pp. 151–160.

Moore, J.C., Vrolijk, P., 1992. Fluids in accretionary prisms. Reviews of Geophysics 30, 113–135.

Moore, J.C., Brown, K.M., Horath, F., Cochrane, G., MacKay, M., Moore, G., 1991. Plumbing accretionary prisms: effects of permeability variations. Philosophical Transactions of the Royal Society A335, 275–288.

Morrow, C.A., Shi, L.Q., Byerlee, J.D., 1984. Permeability of fault gouge under confining pressure and shear stress. Journal of Geophysical Research 89, 3193–3200.

Paterson, M.S., 1990. Rock deformation experimentation. In: Duba, A.G., Durham, W.B., Handin, J.W., Wang, H.F. (Eds.), The Brittle–Ductile Transition in Rocks—The Heard Volume, Geophysical Monograph of the American Geophysical Union, 56, pp. 187–194.

Rice, J.R., 1992. Fault stress states, pore pressure distributions, and the weakness of the San Andreas fault. In: Evans, B., Wong, T.-f. (Eds.), Earthquake Mechanics and Transport Properties of Rocks. Academic Press, London, pp. 475–503.

Screaton, E.J., Wuthrich, D.R., Dreiss, S.J., 1990. Permeabilities, fluid pressures, and flow rates in the Barbados Ridge complex. Journal Geophysical Research 95, 8997–9007.

Stephenson, E.L., Maltman, A.J., Knipe, R.J., 1994. Fluid flow in actively deforming sediments: 'dynamic permeability' in accretionary prisms. In: Parnell, J. (Ed.), Geofluids: Origin, Migration and Evolution of Fluids in Sedimentary Basins, Geological Society Special Publication, 78, pp. 113–125.

Taylor, E., Leonard, J., 1990. Sediment consolidation and permeability at the Barbados forearc. In: Moore, J.C., Mascle, A., et al. (Eds.), Proceedings of the Ocean Drilling Program, Scientific Results, 110. College Station, TX (Ocean Drilling Program), pp. 289–308.

Tobin, H., Moore, J.C., 1997. Variations in ultrasonic velocity and density with pore pressure in the décollement zone, northern Barbados ridge accretionary prism. In: Shipley, T.H., Ogawa, Y., Blum, P., Bahr, J.M. (Eds.), Proceedings of the Ocean Drilling Program, Scientific Results, 156. College Station, TX (Ocean Drilling Program), pp. 125–135.

Tobin, H.J., Moore, J.C., Moore, G.F., 1994. Fluid pressure in the frontal thrust of the Oregon accretionary prism: Experimental constraints. Geology 22, 979–982.

Walsh, J.B., 1981. Effect of pore pressure and confining pressure on fracture permeability. International Journal of Rock Mechanics 18, 429–435.

Walsh, J.B., Brace, W.F., 1984. The effect of pressure on porosity and the transport properties of rock. Journal of Geophysical Research 89, 9425–9431.

Wood, D.M., 1990. Soil Behaviour and Critical State Soil Mechanics, 1st edn. Cambridge University Press, Cambridge.

Zwart, G., Brückmann, W., Moran, K., MacKillop, A.K., Maltman, A.J., Bolton, A., Vrolijk, P., Miller, T., Gooch, M.J., Fisher, A., 1997. Evolution of hydrogeologic properties of the Barbados accretionary prism: A synthesis of Leg 156 results. In: Shipley, T.H., Ogawa, Y., Blum, P., Bahr, J.M. (Eds.), Proceedings of the Ocean Drilling Program, Scientific Results, 156. College Station, TX (Ocean Drilling Program), pp. 303–310.

Zhang, S., Paterson, M.S., Cox, S.F., 1994. Porosity and permeability evolution during hot isostatic pressing of calcite aggregates. Journal of Geophysical Research 99, 15741–15760.

Zhang, S., Tullis, T.E., 1998. The effect of fault slip on permeability and permeability anisotropy in quartz gouge. Tectonophysics 295, 41–52.

Zhang, S., Tullis, T.E., Scruggs, V.J., 1999a. Deformation-induced permeability anisotropy in synthetic gouge materials and implications for fluid pressure within fault zones. Journal of Structural Geology 21, 795–806.

Zhang, S., Tullis, T.E., Scruggs, V.J. (1999b) Implications of permeability and its anisotropy in a mica gouge for pore pressures in fault zones. In: Deformation Processes in the Earth's Crust. The Hobbs Volume. Boland, J.N., Ord, A. (Eds.), Tectonophysics, in press.